

**Investigation of Charging and Discharging Process in a
Rotating Latent Heat Storage**

by

See Itt Ping

16335

Dissertation submitted in partial fulfilment of

the requirements for the

Bachelor of Engineering (Hons)

Mechanical Engineering

JANUARY 2016

Universiti Teknologi PETRONAS

Bandar Seri Iskandar

32610 Tronoh

Perak Darul Ridzuan

CERTIFICATION OF APPROVAL

Investigation of Charging and Discharging Process in a Rotating Latent Heat Storage

by

See Itt Ping

16335

A project dissertation submitted to the

Mechanical Engineering Programme

Universiti Teknologi PETRONAS

In partial fulfilment of the requirements for the

Bachelor of Engineering (Hons)

Mechanical Engineering

Approved by,

(Dr. Jundika Candra Kurnia)

Universiti Teknologi PETRONAS

Bandar Seri Iskandar

32610 Tronoh

Perak Darul Ridzuan

January 2016

CERTIFICATION OF ORIGINALITY

This is to certify that I am responsible for the work submitted in this project, that the original work is my own except as specified in the references and acknowledgements, and that the original work contained herein have not been undertaken or done by unspecified sources or persons.

See Itt Ping

ABSTRACT

Renewable energy has become increasingly popular to ease the global reliance on fossil fuels. Among the emerging renewable energies, solar energy is one of the favourable ones. However, the intermittent nature of solar energy has hindered the wide application of it. Energy storage is required to improve the reliability of this energy source. Among the energy storage, latent heat thermal energy storage (LHTES) is desirable due to its capability to store a large amount of energy with minimum temperature rise. However, poor heat transfer performance is the drawback of the LHTES system. Rotation of LHTES system is proposed to alleviate this situation. In this study, rotation of an LHTES system is examined numerically. The heat transfers between the heat transfer fluid (HTF) and the phase change material (PCM) is solved using computational fluid dynamics (CFD). The results reveal that the rotating LHTES system improves the heat transfer performance. Further analysis of the results discloses that low rotational speed offers the best improvement in heat transfer performance during charging and discharging process. Nevertheless, further research and experimentation are needed to determine the optimum rotational speed and also a commercially viable design for rotating LHTES system.

ACKNOWLEDGEMENT

I express my gratitude to all parties for guidance and advises which helped me to successfully complete my Final Year Project.

First and foremost, my sincere gratitude goes to my supervisor, Dr. Jundika Candra Kurnia for his continuous guidance and teaching throughout this project. His advice has helped me to navigate through the challenges of this project.

In addition, I extend my appreciation to Universiti Teknologi PETRONAS (UTP) through its grant, Short Term Interval Research Fund (STIRF); grant number: 0153AA-D55 for funding this project till completion. I am also grateful for the facilities UTP has provided.

Special thanks to my examiner, Associate Professor Dr. Syed Ihtsham Ul-Haq Gilani for his guidance and teaching in rectifying my mistakes.

Lastly, thanks to my family and friends for their support and encouragement throughout this project.

TABLE OF CONTENTS

CERTIFICATION OF APPROVAL	II
CERTIFICATION OF ORIGINALITY	III
ABSTRACT	IV
ACKNOWLEDGEMENT	V
CHAPTER 1: INTRODUCTION	1
1.1 Background	1
1.2 Problem Statement	3
1.3 Objective	4
1.4 Scope of Studies	4
CHAPTER 2: LITERATURE REVIEW	6
2.1 Latent Heat Thermal Energy Storage (LHTES)	6
2.2 LHTES Heat Transfer Enhancement Methods	7
2.3 Phase Change Material (PCM)	9
2.4 Heat Transfer Fluid (HTF)	11
2.5 Applications of LHTES System	11
2.6 Heat Transfer Mechanism	12
CHAPTER 3: METHODOLOGY	13
3.1 Project Methodology	13
3.2 Project Flow Diagram	17
3.3 Governing Equations	18
3.3.1 Heat transfer fluid	18
3.3.2 Phase change material	18
3.3.3 Constitutive relations	19
3.4 Heat Stored in the LHTES System	20
3.5 Key Milestone & Gantt Chart	21
CHAPTER 4: RESULTS AND DISCUSSION	23
4.1 Mesh Independence Test	23
4.2 Validation of Numerical Solution	24

4.3	Charging & Discharging Cycle	25
4.4	Effect of Orientation.....	26
4.5	Effect of Rotational Speed	30
4.6	Rate of Heat Transfers.....	36
CHAPTER 5: CONCLUSION AND RECOMMENDATION		38
REFERENCE.....		40

List of Figures

Figure 1.1: Distribution of solid–liquid interfaces when liquid fraction is 0.5 for (a) without natural convection and (b) with natural convection [12].	3
Figure 2.1: The comparison of the sensible heat thermal energy storage (SHTES) and LHTES mechanism.	6
Figure 2.2: Different PCM packaging configurations for heat transfer enhancement [3].	8
Figure 2.3: Categorization of PCMs [3].	10
Figure 3.1: The experimental prototype proposed for the study of rotating LHTES system.	13
Figure 3.2: The mesh used to study the rotating LHTES system.	14
Figure 3.3: The proposed experimental prototype developed for the study of rotating LHTES system.	16
Figure 3.4: Project Flow Chart.	17
Figure 3.5: Key Milestones	21
Figure 4.1: Mesh Independent Test.	23
Figure 4.2: Validation against Lacroix [13].	24
Figure 4.3: A shell-and-tube LHTES unit in (a) horizontal orientation, (b) vertical orientation and (c) horizontal orientation with rotation. PCM is stored in the shell (white) while HTF is allowed to flow into the tube (blue).	25
Figure 4.4: Graph of liquid fraction against flow time for horizontal steady, vertical with bottom inlet and vertical with top inlet.	26
Figure 4.5: Liquid fraction of horizontal steady after 1 hour of charging.	27
Figure 4.6: Liquid fraction of vertical steady with bottom inlet after 1 hour of charging.	27
Figure 4.7: Liquid fraction of vertical steady with top inlet after 1 hour of charging.	27

Figure 4.8: Liquid fraction of horizontal steady after 30 minutes of discharging. ...	29
Figure 4.9: Liquid fraction of vertical steady with bottom inlet after 30 minutes of discharging.	29
Figure 4.10: Liquid fraction of vertical steady with top inlet after 30 minutes of discharging.	29
Figure 4.11: Graph of liquid fraction against flow time for horizontal steady, horizontal rotating at 0.25 rpm, horizontal rotating at 0.5 rpm and horizontal rotating at 1 rpm.	30
Figure 4.12: Liquid fraction of horizontal steady after 30 minutes of charging.	31
Figure 4.13: Liquid fraction of horizontal with 0.25 rpm after 30 minutes of charging.	31
Figure 4.14: Liquid fraction of horizontal with 0.5 rpm after 30 minutes of charging.	32
Figure 4.15: Liquid fraction of horizontal with 1 rpm after 30 minutes of charging.	32
Figure 4.16: Liquid fraction of horizontal with 0.25 rpm after 1 hour of charging.	33
Figure 4.17: Liquid fraction of horizontal with 0.5 rpm after 1 hour of charging.	33
Figure 4.18: Liquid fraction of horizontal with 1 rpm after 1 hour of charging.	33
Figure 4.19: Liquid fraction of horizontal with 0.25 rpm after 30 minutes of discharging.	35
Figure 4.20: Liquid fraction of horizontal with 0.5 rpm after 30 minutes of discharging.	35
Figure 4.21: Liquid fraction of horizontal with 1 rpm after 30 minutes of discharging.	35
Figure 4.22: Time taken for charging and discharging process to be completed for all 6 cases.	36

List of Tables

Table 2.1: Properties for PCMs as energy storage materials [3].	10
Table 3.1: Dimensions of proposed experimental prototype.	14
Table 3.2: Thermophysical properties of PCM (n-octadecane).	15
Table 3.3: Boundary conditions of the rotating LHTES simulation.	15
Table 3.4: Project Gantt Chart & Key Milestones.	22
Table 4.1: Heat transfer rates for different cases.	37

CHAPTER 1: INTRODUCTION

1.1 Background

By the year 2040, global energy demand is set to increase by one-third [1], and energy-related CO₂ emissions are predicted to be 16% more [2] as reported in the ‘World Energy Outlook 2015’ and ‘World Energy Outlook 2015 Factsheet’ published by the International Energy Agency (IEA). In order to mitigate environmental problems associated with energy-related CO₂ emission and to reduce our global reliance on fossil fuels, the development of renewable energy technologies has been intensified.

One of the popular options among the numerous types of renewable energy sources is solar energy [3]. Solar photovoltaic (PV) and concentrated solar power (CSP) are the two major technologies used to produce solar energy. The CSP systems consist of a field of solar collectors, receivers, and a power block [4]. Solar energy is directly converted to electricity with the use of PV cells in the PV systems while the solar collectors of the CSP systems concentrate sunlight to the receiver to yield a tremendous amount of heat. This heat is then transported to a power block for power generation with the aid of a heat transfer fluid (HTF) [4]. On the other hand, commercial solar PV systems have lower energy conversion efficiency when compared to CSP systems [3].

Renewable energy technologies are often accompanied with reliability issues. The reason is that renewable energy source often depends on the climate as its source of energy. For example, wind turbines rely on the wind to spin its rotors; PV and CSP need the sunny weather to generate electricity and collect heat. On top of that, renewable energy technologies losses its ability to generate energy once these resources are absent. Therefore, renewable energy technologies can be view as intermittent which subsequently reduces its attractiveness as an energy solution.

Nevertheless, reliability issues of renewable energy technologies can be overcome by integrating it with an energy storage system. Many types of energy storage system are being researched and developed, e.g. chemical energy storage, electrical energy storage, electrochemical energy storage, thermal energy storage (TES), mechanical energy storage [5]. Yet, a deeper assessment reveals that most of them are either cost ineffective or has low effective energy storage or both. Nonetheless, compared to other energy storage technologies, TES system has relatively lower capital expenditures and high round-trip efficiency [6]. Round-trip efficiency is defined as the ratio of the energy output to the energy input in an energy storage system [6]. Hence, the higher the round-trip efficiency, the lower the energy wastage and the more efficient the storage system is.

CSP system equipped with huge TES system are capable of dispatching electrical power during nightfall. Hence, CSP system coupled with TES system is preferred to deliver electricity to the grid at large scale (>100 MW) [3]. The European Solar Thermal Electricity Association and Greenpeace estimate in the Advanced scenario of CSP Global Outlook 2009 (an IEA SolarPACES programme) that, CSP global capacity will reach 1500 GW by 2050 [7].

TES system accumulates thermal energy in the storage medium by means of heating or cooling. This energy is then used for heating and cooling applications or power generation at a later time [8].

Among the types of TES available, sensible heat thermal energy storage (SHTES) system is most commonly used [9]. SHTES system makes use of a storage medium with high specific heat capacity and increases the temperature of the storage medium in order to store thermal energy. The temperature of the storage medium rises throughout charging process (storage) and falls in the discharging process (release) [5].

Nevertheless, latent heat thermal energy storage (LHTES) system is more favourable because it stores energy with minimal temperature rises and thus minimum energy losses. This is achievable as the LHTES system accumulates heat through the phase change process of the storage medium also known as the phase change material

(PCM). It takes advantage of the storage material when it phases change either from solid state to liquid state or liquid state to gas state or vice versa to stored heat [8]. The PCM will either absorb or release heat based on the type of phase change it experience [5].

1.2 Problem Statement

Despite its large energy storage capacity, latent heat thermal energy storage (LHTES) system are often accompanied with low heat transfer performance [9]–[11]. This results in the LHTES system requiring a longer time to be fully charged. The mode of heat transfer in the LHTES is a combination of conduction, convection, and radiation. However, natural convection has a strong influenced on the heat transfer performance of the LHTES.

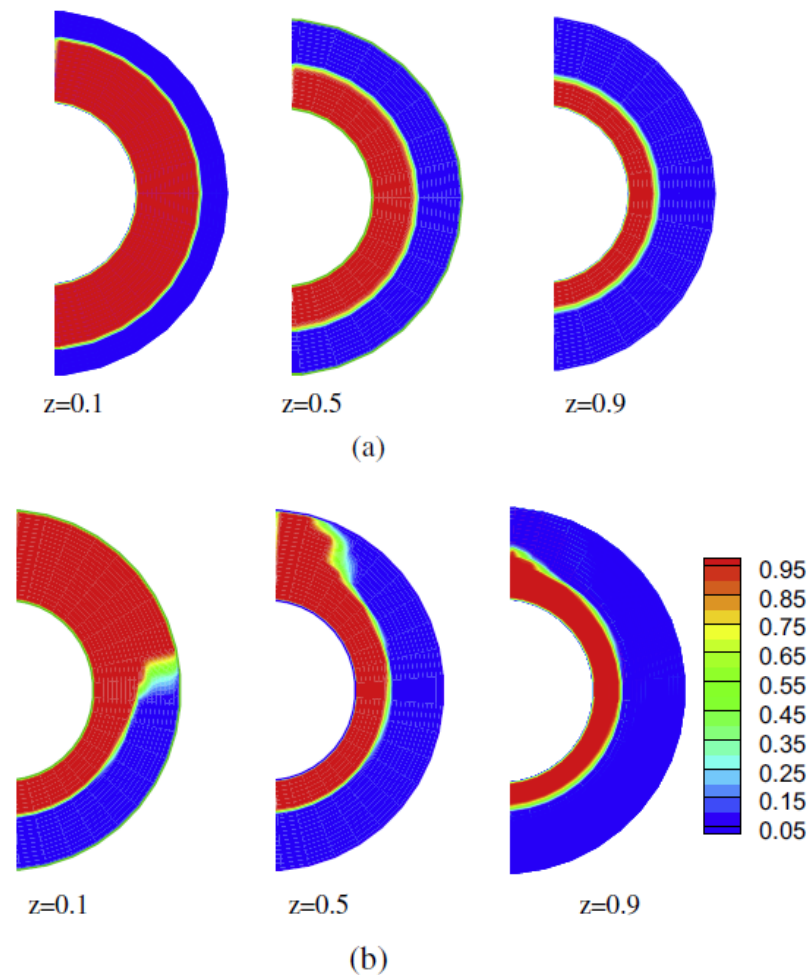


Figure 1.1: Distribution of solid–liquid interfaces when liquid fraction is 0.5 for (a) without natural convection and (b) with natural convection [12].

Tao and He [12] studied the effect of natural convection on an LHTES system. They found that natural convection causes non-uniformity in the LHTES processes as illustrated in **Figure 1.1**. **Figure 1.1** shows the effect of natural convection on solid-liquid interfaces in different cross-section along the axial direction of a shell-and-tube LHTES system when the total PCM melting fraction is 0.5. PCM is stored in the shell while HTF is allowed to flow into the tube. The length of the shell-and-tube container is denoted as z . The uneven solid-liquid interface and liquid fraction distribution in the cross-sectional area of the system are caused by natural convection [12]. By rotating the LHTES system, it is anticipated that the effects of natural convection in the system can be more uniform in the cross-section. Therefore, by rotating the LHTES system, it would enhance its heat transfer performance.

1.3 Objective

The objectives of this project are as the following:

- 1.3.1 To conduct numerical studies of a rotating LHTES; and
- 1.3.2 To investigate the heat transfer performance of the rotating LHTES and its key parameters.

1.4 Scope of Studies

This study focuses on the comparison of the charging and discharging process of different latent heat thermal energy storage (LHTES) systems, i.e. stationary LHTES system and rotating LHTES system. The LHTES system used in this study is a simple shell-and-tube type. The primary simulation approach is computational fluid dynamic (CFD) technique via ANSYS Fluent solver. The state of the heat transfer fluid in the tubes is laminar flow with an inlet velocity of 0.1 m/s.

In the study of stationary LHTES system, three different orientations of LHTES system is investigated. The orientations investigated are horizontal steady, vertical steady with inlet at the top, and vertical steady with inlet at the bottom. On the other hand, the study of rotating LHTES system focuses on the horizontal orientation. The rotating LHTES system rotates around its axis. Three different rotational speeds

of LHTES system is investigated. The rotational speeds investigated are 0.25 rpm, 0.5 rpm, and 1 rpm. Therefore, a total of six CFD simulation is carried out.

The PCM used in this study is paraffin wax (n-octadecane). It was chosen due to its availability and low cost. On the other, n-octadecane is chemically stable, safe and non-reactive. It has a high heat of fusion and melts congruently around the range of 27.7 °C [13], [14].

The HTF used in this project is water as it is readily available, has a low freezing point and has high specific heat capacity [15], [16]. Water also has acceptably small corrosion rate.

The preliminary CFD results is validated against a numerical model for a shell-and-tube LHTES unit developed by Lacroix [13].

CHAPTER 2: LITERATURE REVIEW

2.1 Latent Heat Thermal Energy Storage (LHTES)

LHTES system utilizes phase change material (PCM) to store thermal energy. This system takes advantage of the PCM to store thermal energy when it undergoes phase change either from solid state to liquid state or liquid state to gas state or vice versa [8]. The PCM will either absorb or release heat based on the type of phase change it undergoes [5].

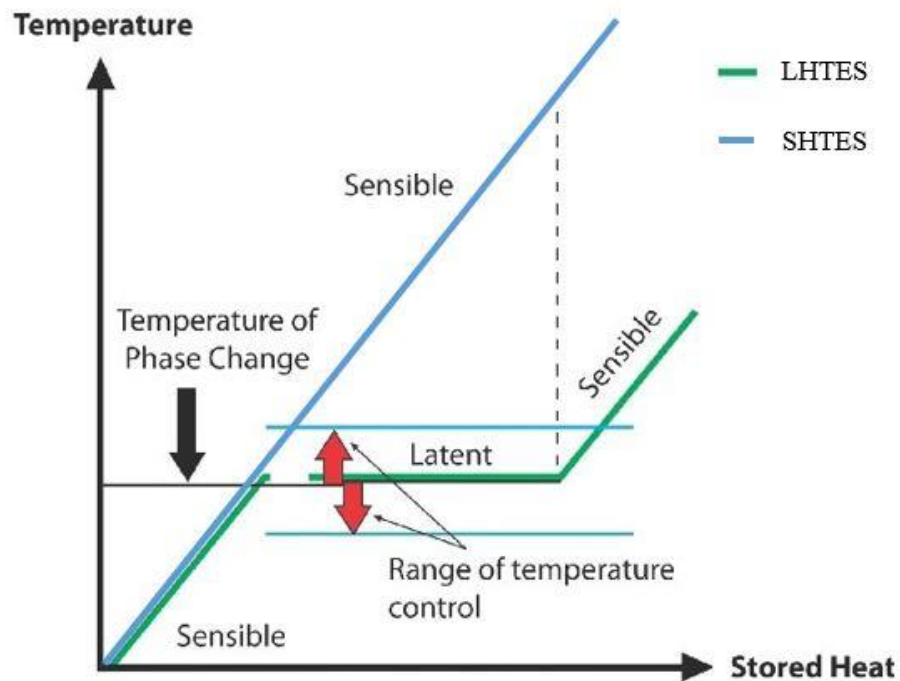


Figure 2.1: The comparison of the sensible heat thermal energy storage (SHTES) and LHTES mechanism.

Storage material for sensible heat thermal energy storage (SHTES) system and LHTES system has been studied the most. These studies reveal that LHTES system

has significantly smaller storage volume than the SHTES system while still maintaining the same storage capacity. This is achieved through the usage of PCMs. By using PCM, charging and discharging process in the LHTES system are almost isothermal as shown in **Figure 2.1**. Isothermal temperature is important as it reduces the heat loss in the system. Furthermore, it is also important to accommodate solar field equipment and also the thermal power Rankine cycles [3], [5], [9]–[12], [17]. Phase change latent heat governs most of the storage capacity of an LHTES system resulting in more than ten times larger storage capacity than SHTES system. Thus, the design of LHTES system can be smaller, compact and cheaper than SHTES system [3].

The three basic components of all LHTES system are a heat storage material (PCM) that go through a phase transition in the system's operating temperature range and where the heat added is stored as the latent heat of fusion; a container for storing the PCM and a heat exchanging surface for transferring heat from the heat transfer fluid (HTF) to the PCM and from the latter to the heat sink [3], [6], [18].

Despite LHTES being more superior to SHTES, it does come with some drawback. Low thermal conductivity, density variation, and stability of properties under extended charging and discharging and sometimes phase segregation and sub-cooling of the PCM are some of the practical difficulties of LHTES system [9]. Sub-cooling is not desirable as it decreases the usability of PCMs and can also completely stop heat recovery in serious cases [3]. However, poor heat transfer performance is one of the main problems face by the high energy storage LHTES system [11].

2.2 LHTES Heat Transfer Enhancement Methods

Various heat transfer enhancement has been introduced to the LHTES system to improve its thermal conductivity. The use of fins in different configuration has been proven to be effective means of improving heat transfer during charging and discharging of the LHTES system. Other methods propose by researchers include introducing a metal matrix into a PCM, using PCM spread with high conductivity particles and micro-encapsulation of PCM [9], [11].

The novelty of micro-encapsulation of PCM is to increase the surface area that the PCM interacts with the HTF. Therefore, heat transfer area of the PCM is increased. Micro-encapsulation also reduces the reactivity of the PCM with the outside environment and enables the PCM to withstand frequent changes in the volume during phase change [19].

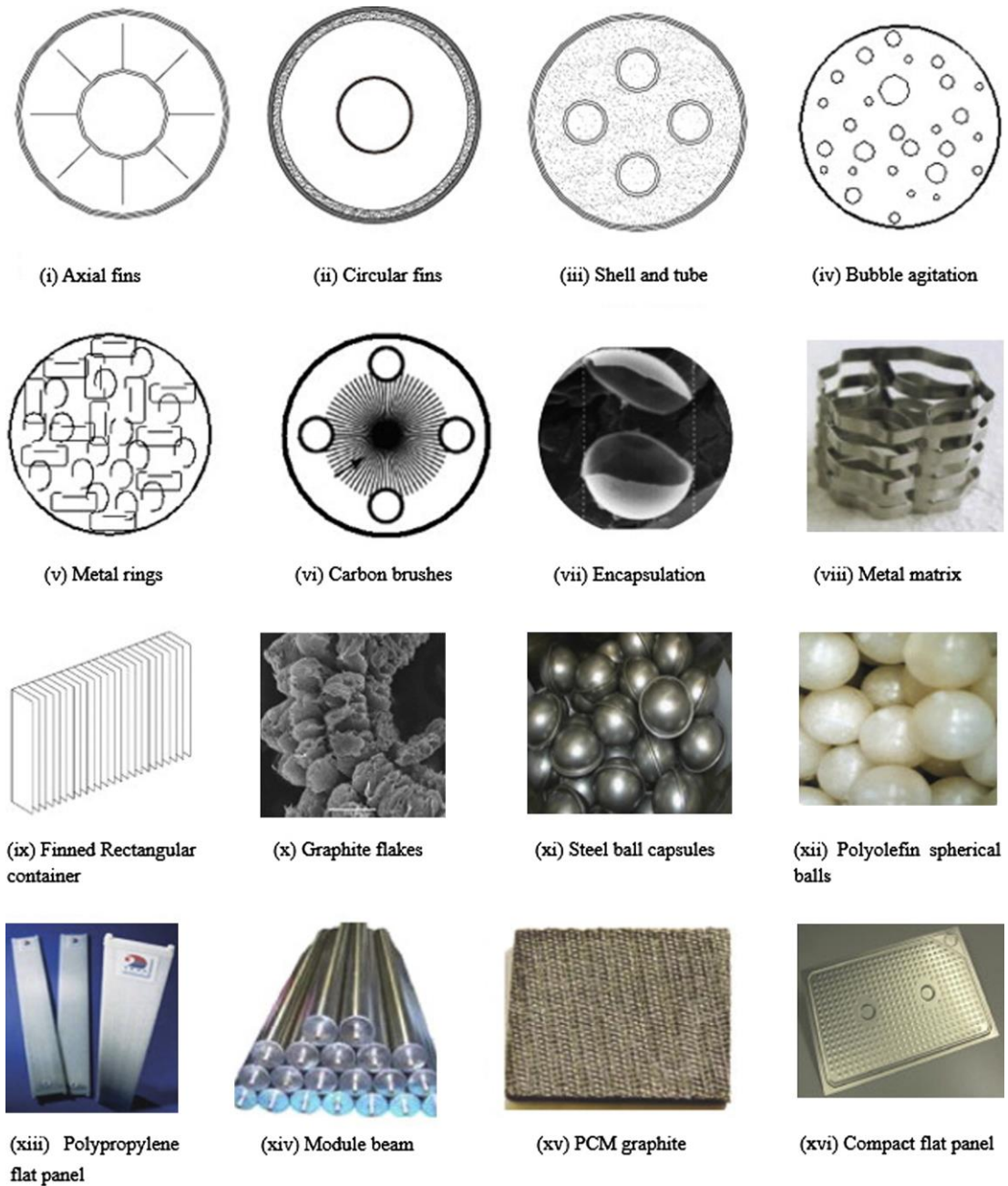


Figure 2.2: Different PCM packaging configurations for heat transfer enhancement [3].

Bubble agitation is achieved by adding a small amount of water with molten paraffin into a tube. The tube is then evacuated by a vacuum pump so that saturation temperature of the water inside the tube is approximately the same to the phase change temperature of the PCM. During the phase change, steam bubbles are generated inside the PCM to promote heat transfer [3].

Carbon fibres brushes are developed to improve thermal conductivities of PCMs. Low volume fraction brushes were dispersed in the PCMs as the volume fraction of the fibres is easily controlled. The brushes are then packed together with PCMs into cylindrical capsules [3].

The idea of the micro-encapsulation of PCM technique is to boost the heat transfer area of the PCM. This will lead to better heat transfer with the HTF. Heat transfer area of 300 square meters per cubic meter can be achieved with the use of PCM capsules with a radius of 10 millimetres. Capsule size varies with different techniques of encapsulation. For high-temperature application, metallic encapsulation of PCM is desired while in low-temperature application, plastic encapsulation is normally preferred [3].

2.3 Phase Change Material (PCM)

Phase change materials and storage materials that undergo phase change to store thermal energy. Suitable materials for LHTES must have a large latent heat and high thermal conductivity. Besides that, they should possess a melting temperature in the operation range of LHTES, melt consistently with little sub-cooling and be chemically stable, economically cheap, harmless and non-corrosive. The melting temperature of a PCM are usually the main selection criteria. Materials with melting temperature in the range of 15°C to 90°C are the most studied and are usually incorporated into solar heating or heat load levelling applications [9]. Desired properties of storage medium suitable as a PCM is detailed in **Table 2.1**.

PCM materials that were studied are hydrated salts, paraffin waxes, fatty acids and eutectics of organic and non-organic compounds as shown in **Figure 2.3**. *Eutectics* is defined as the melting point of a mixture of substances in a fixed ratio at a single

temperature that is lower than the melting points of its individual components or of any other mixture of them.

Table 2.1: Properties for PCMs as energy storage materials [3].

Thermal	Chemical	Physical	Economical
1. Phase change temperature suits application	1. Stability	1. Low-density variation	1. Cheap
2. High enthalpy change	2. No phase separation	2. High Density	2. Abundant
3. High thermal conductivity in both liquid and solid phases	3. Compatibility with container material	3. Small or no sub-cooling	3. Available
	4. Non-toxic, non-flammable, non-polluting		

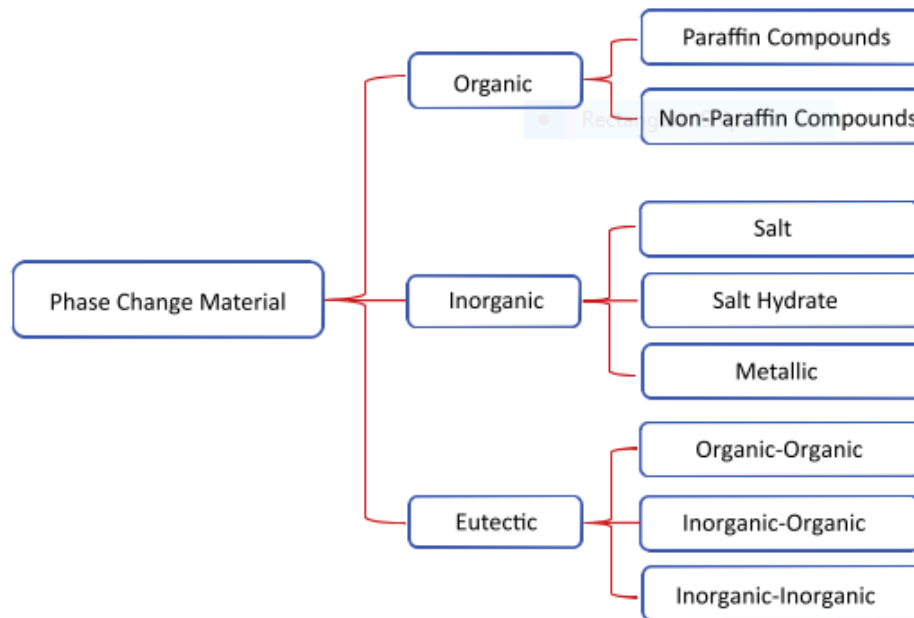


Figure 2.3: Categorization of PCMs [3].

The melting point of commercial paraffin waxes is between 23°C to 68°C. It is low-cost with reasonable thermal storage densities (~200 kJ/kg or 150 MJ/m³). It experiences negligible sub-cooling and are chemically stable with no phase segregation. Still, commercial paraffin waxes have low thermal conductivity (~0.2

W/m.°C), which limits their applications. Studies mainly surround commercial paraffin waxes which melt around 55°C [9].

Gibbs and Hassan [20] used differential scanning calorimetry (DSC) to investigate the behaviour of storage materials that undergo solid-liquid phase transitions. They discovered that paraffin wax did not supercool and its heat transfer performance is not affected by the thermal cycling or interaction with metal.

2.4 Heat Transfer Fluid (HTF)

HTFs are used to add and remove heat to / from the PCM. Air, water / steam, mineral / synthetic oils and inorganic molten salts are some of the commercial HTFs used in solar power plants. HTFs must be well-suited with the container materials, storage medium and capable of functioning in the required temperature range [6]. The recommended characteristics of HTFs are high heat capacity, good thermal stability, low freezing point, low viscosity and low corrosion rate to metal alloys of pipes used to transport the HTFs. Another critical criterion for industrial applications would be low cost [3].

2.5 Applications of LHTES System

LHTES system can be used with a solar power generation system as well as industrial waste heat recovery system. Research on implementation of LHTES system in solar power generation system is underway. Solar thermal energy is used to melt the PCM of the LHTES system with the aid of the HTF. LHTES system releases its thermal energy to produce steam during nighttime or cloudy weather conditions. Obstacles with the application of LHTES system in the solar power generation system are the suitability of PCM and low thermal conductivity. PCM used for solar power generation should have a melting point in the range of 200°C to 300°C depending on the type of power cycle and solar power generation plant adopts [19]

Lately, a waste heat transportation system based on the LHTES system was proposed. In this system, melting of the PCMs recovers industrial waste heat and distributes to office buildings, hospital, hotels and etc. Recovered heat can be used for

the building heating, ventilation, and air conditioning. In the case of air conditioning, hot water produced from the LHTES system is used to operation an adsorption chiller. Then, the adsorption chiller produces chilled water for the air conditioning units. At the moment, LHTES system used for industrial waste heat recovery are limited to a low temperature range (200°C) while the huge quantity of waste heat over 300°C can be potentially recovered. Research into a high temperature waste heat recovery is ongoing [19].

2.6 Heat Transfer Mechanism

Heat transfer occurs when a temperature difference exists between 2 mediums until a temperature equilibrium is achieved. There are 3 modes of heat transfer, i.e. conduction, convection, and radiation. Conduction is the transfer of energy from high-temperature medium to low temperature medium due to interactions between particles. Conduction can take place in solids, liquids, or gases. The heat transfer through conduction is affected by the medium's thermal conductivity. The higher the thermal conductivity, the easier heat is transferred across the medium and vice versa [15].

Energy transfer due to the combined effects of conduction and fluid motion is convection. Convection takes places when the temperature difference is present between a solid surface and its neighboring liquid or gas which are in motion. Heat transfer through convection increases when the fluid flows increases [15].

Forced convection occurs when fluids are forced to flow due external forces acting on it. Contrary to that, natural convection occurs when the effects of the temperature difference in a fluid cause variation in its density. This will induce a buoyancy force which acts on the fluid. Hotter fluids will rise while cooler fluids will sink. Heat transfer during the phase change of a fluid are regarded as convection as the fluid motions are induced [15].

CHAPTER 3: METHODOLOGY

3.1 Project Methodology

Before initiating this study, a literature review has been conducted. Previous studies are reviewed to gain some basic understanding of this topic. Literature review is also done to spot related work performed within this area and gather vital information on how the numerical were executed. Additionally, literature review is important to determine gaps in knowledge that require additional research. This will help the identification of the problem statement, objective, and scope of study of this project.

Next phase of the project is the numerical studies. Finite volume method via ANSYS Fluent 15.0 is used in this project. For this project, ANSYS Fluent 15.0 is selected as it was the one of the licensed computational fluid dynamics (CFD) software available in UTP. The numerical studies of this project can be divided into 3 parts, modeling, meshing, and simulation.

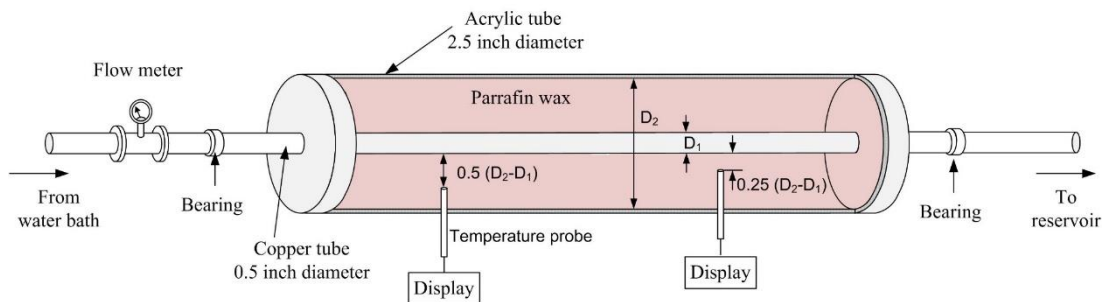


Figure 3.1: The experimental prototype proposed for the study of rotating LHTES system.

The model of this project is formulated based on the proposed experimental prototype. **Figure 3.1** shows the proposed experimental prototype which is a basic

shell-and-tube LHTES system. The dimensions of the proposed experimental prototype are given in **Table 3.1**. However, due to time constraint and technical issues with the experimental prototype, the experimental method has since been abandoned. This project used AutoCAD 2016 Student Version to create the model. The geometrical modelling is constructed based on the interior fluid body of shell-and-tube configuration.

Table 3.1: Dimensions of proposed experimental prototype.

Parameters	Dimensions (m)
Diameter Acrylic Tube	0.0258
Outer Diameter Cooper Tube	0.0158
Inner Diameter Cooper Tube	0.0127
Length	1

After modelling is completed, the model is imported into ANSYS Workbench for the meshing stage. The meshing of the model is performed using ANSYS Meshing. **Figure 3.2** shows the mesh used to study the rotating LHTES system. In this figure, the acrylic tube (green) adopts a structured grid with the hexahedron cell shapes while the copper tube (red) utilised a hybrid grid that contain a combination triangular prism cell shapes and hexahedron cell shapes. After meshing is done, the mesh is labelled according to their respective surfaces.

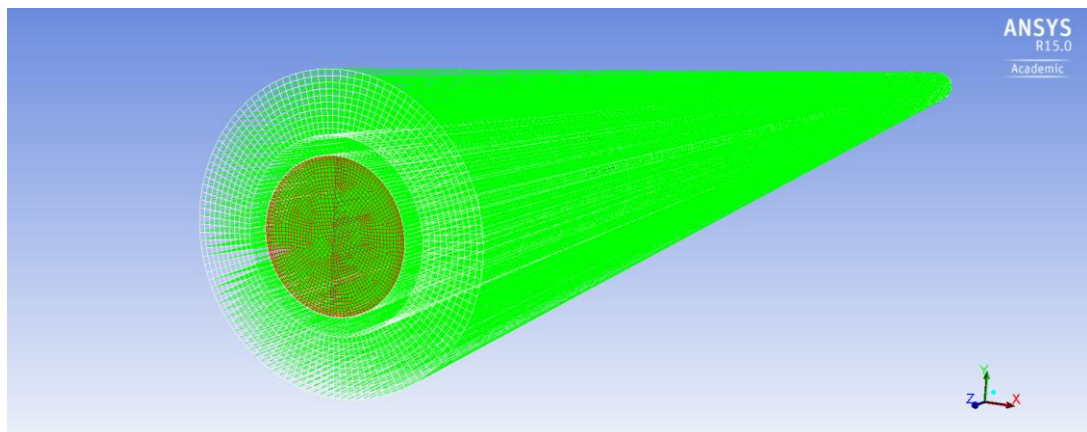


Figure 3.2: The mesh used to study the rotating LHTES system.

After meshing is completed, the numerical simulation may begin. The material properties used in this simulation are written as a user-defined function (UDF) in C language. The UDF is then loaded into the ANSYS Fluent 15.0. **Table 3.2** describe the thermophysical properties of the PCM used in this project. Subsequently, the boundary conditions of the LHTES system as described in **Table 3.3** are applied into the Fluent software. In order to obtain the rotational effect in the simulation Frame Motion in the Cell Zone Condition is turned on and the rotational speed is then specified accordingly in rotation per minute (rpm). Solution initialization is set up with the temperature fix to 295.65K (22.65°C) before running the simulation.

Table 3.2: Thermophysical properties of PCM (n-octadecane).

Parameters	Values	Unit
Melting temperature [13]	300.7	K
	27.7	°C
Enthalpy of fusion [13]	243.5	kJ/kg
Thermal conductivities [13]	0.148	W/m.K
	0.358	
Specific heat capacity (Solid) [21]	1.712	kJ/kg.K

Table 3.3: Boundary conditions of the rotating LHTES simulation.

Components	Boundary Type	Boundary Conditions	
		Charging	Discharging
Wall	Wall	<ul style="list-style-type: none"> • Stationary with no slip condition • No heat flux 	
Inlet	Velocity Inlet	<ul style="list-style-type: none"> • Velocity magnitude = 0.1 m/s <ul style="list-style-type: none"> ○ Reynold number = 1663 (Laminar flow) 	
		<ul style="list-style-type: none"> • Temperature = 305.65K (32.65°C) 	<ul style="list-style-type: none"> • Temperature = 295.65K (22.65°C)
Outlet	Outflow	<ul style="list-style-type: none"> • Flow Rate Weighting = 1 	

The charging process is conducted when the PCM is in the solid state. To start the charging process, hot HTF is passed through the tube. Heat from the HTF is

absorbed and stored in the PCM. The charging process is completed once all of the PCM has completely melted. Meanwhile, the discharging process is carried out right after the completion of charging process. The discharging process ends when all of the PCM has solidified back.

Last but not least, mesh independence test and validation of preliminary results are conducted. Mesh independence test is conducted to evaluate the optimum mesh size to be used in the simulation. This is because the smaller the mesh size used for the simulation, the larger the computational power needed to run the simulation. This will lead to increase in time needed to complete the simulation. Validation is done with the preliminary results to evaluate the accuracy of the simulation results with regards to the actual results. Once both of these are done, the simulation of rotating LHTES system may begin. The results obtained is then analysed and discussed.



Figure 3.3: The proposed experimental prototype developed for the study of rotating LHTES system.

3.2 Project Flow Diagram

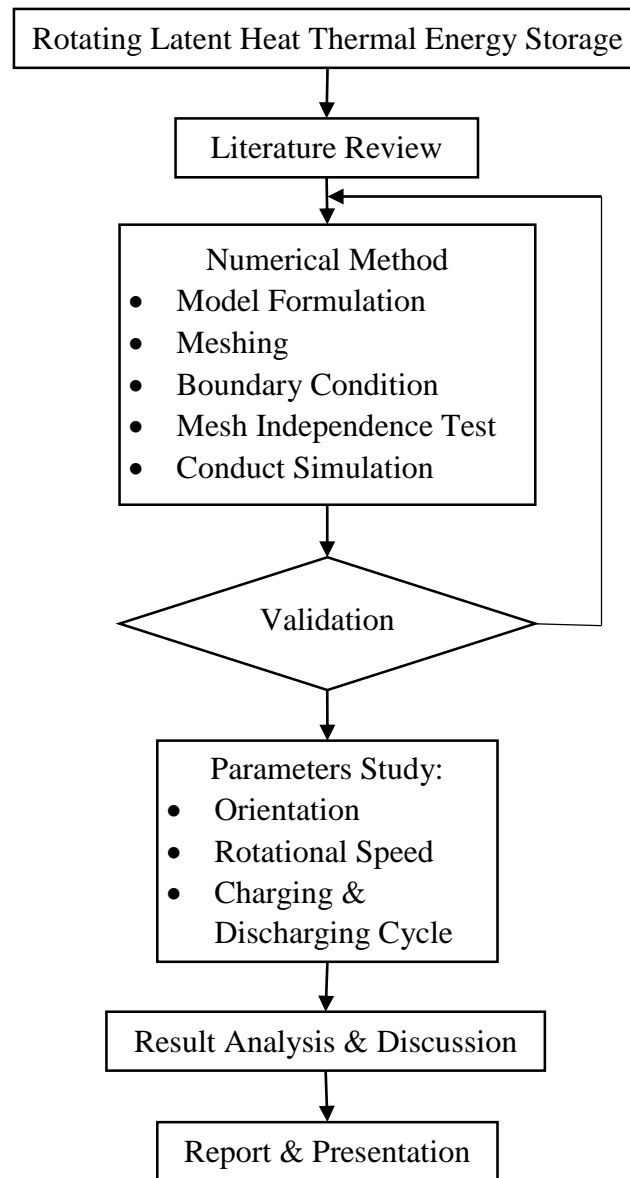


Figure 3.4: Project Flow Chart

Figure 3.4 shows the project flow chart. As observed from the chart, a literature review is conducted first. This followed with the model formulation, meshing and also boundary condition calculation / identification. Once completed, the mesh independence test is done to determine mesh size for the simulation. A trial simulation is run for validation purposes. This is to prove the accuracy of the simulation against the real world scenario. A parameter study is then carried out after validation produces desirable results. After parameter study is completed, its results are then examined and interpreted.

3.3 Governing Equations

3.3.1 Heat transfer fluid

The conservation equations of mass, momentum, and energy of HTF are given by [22]:

$$\frac{\partial \rho_w}{\partial t} + \nabla \cdot (\rho_w \mathbf{u}) = 0 \quad (1)$$

$$\frac{\partial (\rho_w \mathbf{u})}{\partial t} + \nabla \cdot (\rho_w \mathbf{u} \otimes \mathbf{u}) = -\nabla p + \nabla \cdot [\mu_w (\nabla \mathbf{u} + (\nabla \mathbf{u})^T)] \quad (2)$$

$$\frac{\partial}{\partial t} (\rho_w c_{p,w} T) + \nabla \cdot (\rho_w c_{p,w} \mathbf{u} T) = \nabla \cdot (k_w \nabla T) \quad (3)$$

where ρ_w is fluid density,

μ_w is dynamic viscosity,

$c_{p,w}$ is specific heat of HTF and

T is temperature.

Fluid flow and convective heat transfer are taken into consideration.

3.3.2 Phase change material

The conservation equations of mass, momentum, and energy of PCM are given by [22]:

$$\frac{\partial \rho_{pcm}}{\partial t} + \nabla \cdot (\rho_{pcm} \mathbf{u}) = 0 \quad (4)$$

$$\frac{\partial \rho_{pcm}}{\partial t} + \nabla \cdot (\rho_{pcm} \mathbf{u} \otimes \mathbf{u}) = \nabla \cdot \boldsymbol{\sigma} + \rho_{pcm} \mathbf{g} + S_{mom} \quad (5)$$

$$\boldsymbol{\sigma} = -pl + \nabla \cdot [\mu_{pcm} (\nabla \mathbf{u} + (\nabla \mathbf{u})^T)] \quad (6)$$

$$S_{mom} = \frac{(1-\beta)^2}{(\beta^3 + 0.001)} \mathbf{H} \mathbf{u} \quad (7)$$

$$\frac{\partial}{\partial t} (\rho_{pcm} H_{pcm}) + \nabla \cdot (\rho_w \mathbf{u} H_{pcm}) = \nabla \cdot (k_{pcm} \nabla T) \quad (8)$$

where ρ_{pcm} is fluid density of PCM,

\mathbf{u} is fluid velocity,

p is pressure,

μ_{pcm} is dynamic viscosity of PCM,

H is mushy zone constant and

T is temperature.

Fluid flow, heat transfer and phase change processes of PCM are taken into consideration.

3.3.3 Constitutive relations

The thermophysical properties of HTF (water) are expressed as a polynomial function [22].

$$\rho_w = (-3.570 \times 10^{-3})T^2 + 1.88T + 753.2 \quad (9)$$

$$\mu_w = 2.591 \times 10^{-5} \times 10^{\left(\frac{238.3}{T-143.2}\right)} \quad (10)$$

$$k_w = (-8.354 \times 10^{-6})T^2 + (6.53 \times 10^{-3})T - 0.5981 \quad (11)$$

$$c_{p,w} = 4200 \text{ J/kg.K} \quad (12)$$

The thermophysical properties of PCM (paraffin wax) are given by [22]:

$$\rho_{pcm} = \frac{750}{0.001(T-319.15)+1} \quad (13)$$

$$k_{pcm} = \begin{cases} k_{pcm}^{(s)}, & \text{if } T < T_{solidius} \\ k_{pcm}^{(l)}, & \text{if } T > T_{liquidius} \end{cases} \quad (14)$$

$$\mu_{pcm} = 0.001e^{(-4.25+1790/T)} \quad (15)$$

The enthalpy of PCM (paraffin wax) is given by [22]:

$$\Delta h_{pcm} = h_{sensible} + h_{latent} \quad (16)$$

where $h_{sensible}$ is sensible heat of PCM, and h_{latent} is latent heat of PCM.

$$h_{sensible} = h_{pcm}^{ref} + \int_{T_{ref}}^T c_{p,pcm} dT \quad (17)$$

$$h_{latent} = \beta L \quad (18)$$

$$\beta = \begin{cases} 0, & \text{if } T < T_{solidius} \\ \frac{T - T_{solidius}}{T_{liquidius} - T_{solidius}}, & \text{if } T_{solidius} < T < T_{liquidius} \\ 1, & \text{if } T > T_{liquidius} \end{cases} \quad (19)$$

where $c_{p,pcm}$ is specific heat of PCM,

T is temperature,

β is melted mass fraction of PCM and

L is latent heat of PCM.

3.4 Heat Stored in the LHTES System

Using equation 17, sensible heat of PCM is determined.

$$\begin{aligned} h_{sensible} &= h_{pcm}^{ref} + \int_{T_{ref}}^T c_{p,pcm} dT \\ &= c_{p,pcm} T_{ref} + \int_{T_{ref}}^T c_{p,pcm} dT \\ &= (1.712 \text{ kJ/kg. K})(295.65) + \int_{295.65}^{305.65} (1.712 \text{ kJ/kg. K}) dT \\ &= 523.2728 \text{ kJ/kg} \end{aligned}$$

Using equation 18, latent heat of PCM is determined.

$$\begin{aligned} h_{latent} &= \beta L \\ &= (1)(243.5 \text{ kJ/kg}) \\ &= 243.5 \text{ kJ/kg} \end{aligned}$$

The total enthalpy of PCM is given by equation 16:

$$\begin{aligned}\Delta h_{pcm} &= h_{sensible} + h_{latent} \\ &= 523.2728 \text{ kJ/kg} + 243.5 \text{ kJ/kg} \\ &= 766.7728 \text{ kJ/kg}\end{aligned}$$

Since $q = C_p \Delta T = \Delta h$, heat gain by the LHTES system is equal to the enthalpy change during charging process. Therefore, **total heat stored in the LHTES system is 766.78 kJ/kg and is the same for all simulation cases in this project.**

However, the rate of heat transfer is different for all simulation cases in this project. This is because rate of heat transfer is defined as heat transfer over time, $\dot{q} = q/t$ where t represents time taken for the LHTES system to be fully charged.

3.5 Key Milestone & Gantt Chart

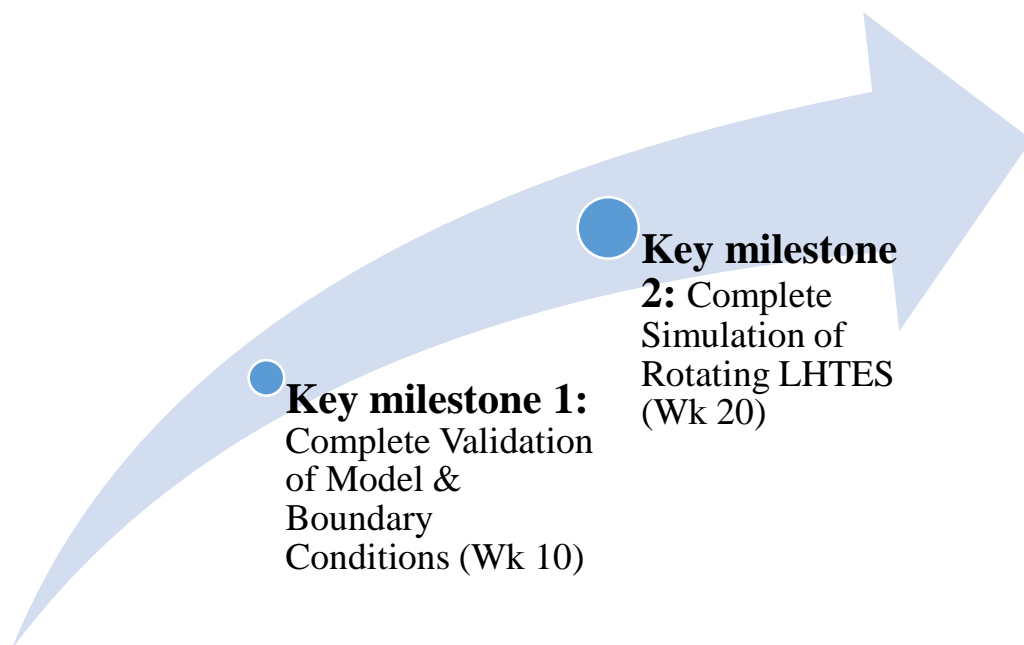


Figure 3.5: Key Milestones

Table 3.4: Project Gantt Chart & Key Milestones.

No.	Activities	1	2	3	4	5	6	7	8	9	10	11	12	13	14	15	16	17	18	19	20	21	22	23	24	25	26	27	28		
1	Background Study & Literature Review			█	█	█	█	█	█	█	█	█	█	█	█	█	█	█	█	█	█	█	█	█	█	█	█	█	█		
2	Modelling and Meshing						█	█																							
3	Validation of Model & Boundary Conditions								█	█	①																				
4	Simulation with ANSYS Fluent											█	█	█	█	█	█	█	█	█	█	②									
5	Evaluation of Key Parameters																						█	█	█						
6	Dissertation Preparation																								█	█	█	█			
7	Viva Preparation																											█	█		
8	Progress Report							█								█							█								

█ FYP1
 █ FYP2

Key Milestone ① : Complete Validation of Model & Boundary Conditions

Key Milestone ② : Complete Simulation of Rotating LHTES

CHAPTER 4: RESULTS AND DISCUSSION

4.1 Mesh Independence Test

Mesh independence test is conducted to make sure that the solution is independent of the mesh resolution. Before starting the simulations, the mesh independence test is conducted to determine the optimum mesh size to be used for the simulation. In CFD, the smaller the mesh size, the more accurate the solution. The optimum mesh would be the largest mesh size that produces similar or approximately close solution to the smaller mesh size. This is because the bigger the mesh size, the lesser the number of cells. **Figure 4.1** shows the comparison between mesh size. From the figure, it is observed that all the mesh size performs similarly during the test. Therefore, the 252,000 cells meshing is chosen for the simulation as it has the least amount of cells and at the same time does not disrupt the simulated solution.

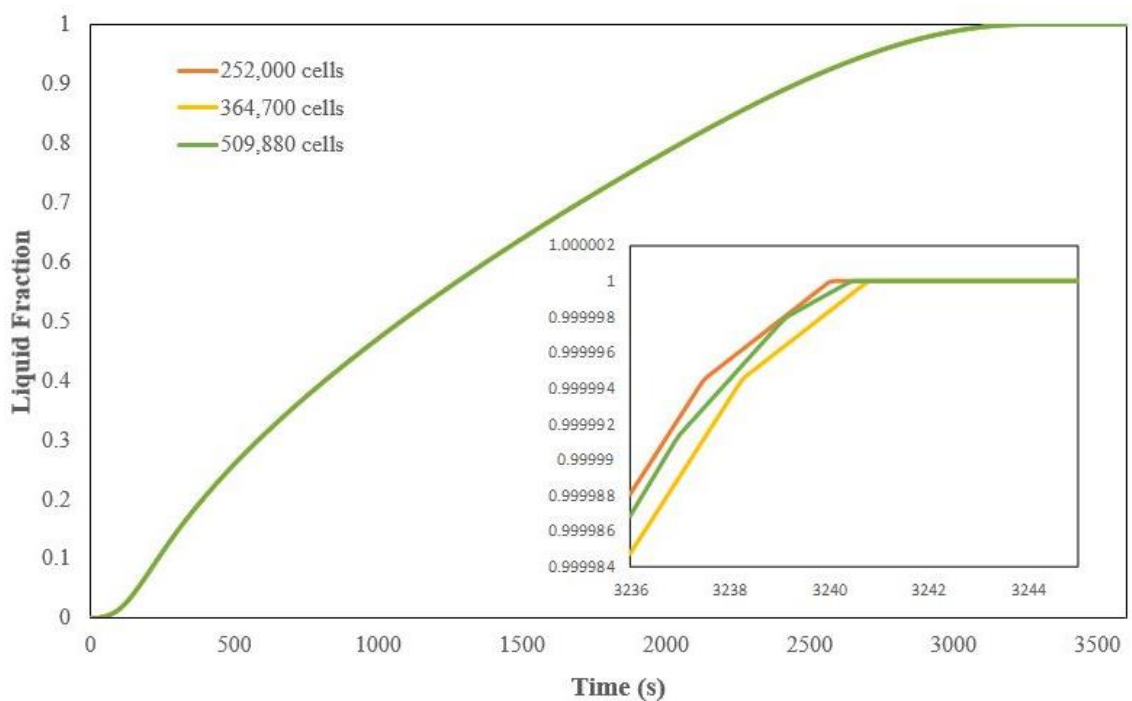


Figure 4.1: Mesh Independent Test

4.2 Validation of Numerical Solution

Lacroix [13] has developed a numerical model for a shell-and-tube latent heat thermal energy storage (LHTES) unit. Lacroix's numerical solution was validated against the experiment conducted by himself. In **Figure 4.2** shows the comparison of the preliminary numerical solution against the numerical and experimental work done by Lacroix. In this figure, T1 represents the temperature at the inlet while T2 represents the temperature at the outlet. The experimental solution is represented by "expt" while the numerical solution is represented by "sim". "Present sim" represents the preliminary numerical solution.

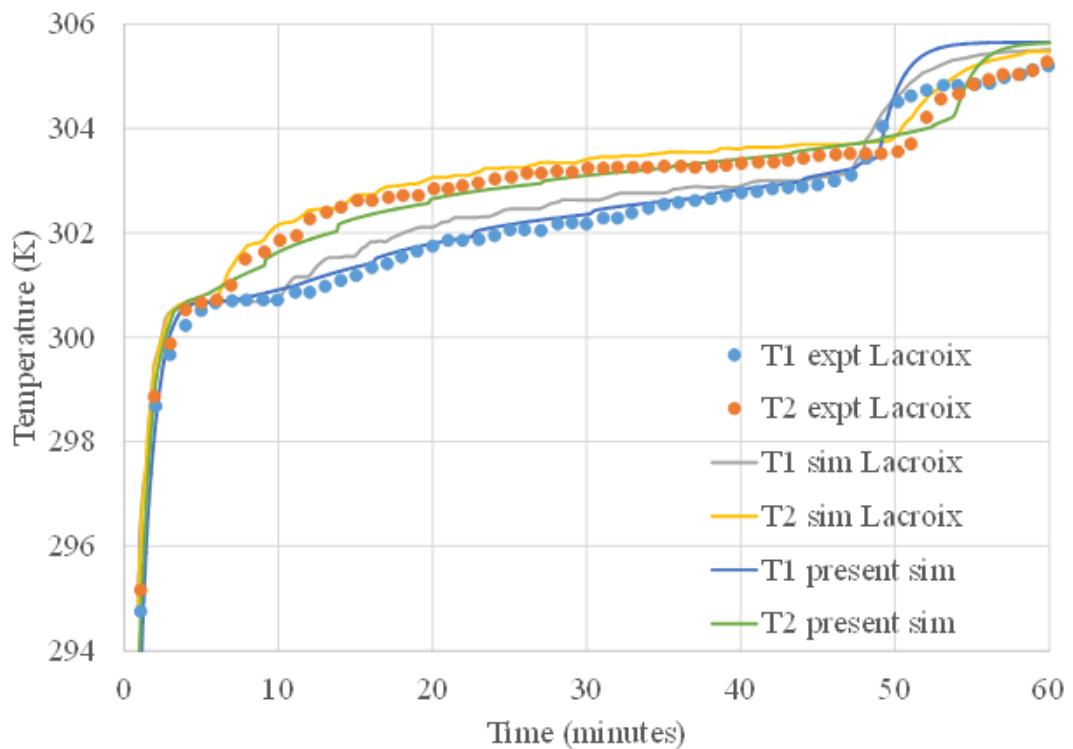


Figure 4.2: Validation against Lacroix [13].

When the temperature profile of the preliminary numerical solution is compared against the numerical solution and experimental solution of Lacroix, it is observed the variation between these 3 temperature profiles are small. The temperature curves of the inlet of the shell-and-tube LHTES is almost similar in all 3 solutions. This is the same at the outlet of the LHTES. This proves that the preliminary numerical solution is approximately accurate to the actual solution.

4.3 Charging & Discharging Cycle

Simulation concerning the effect of orientation of the LHTES system and effect of rotational speed is carried out. In the effect of orientation of LHTES system, three cases were studied namely horizontal steady, vertical steady with an inlet at the top and vertical steady with an inlet at the bottom. Another three cases were studied for the effect of rotational speed. All the three cases are all in a horizontal orientation with different rotational speed, i.e. 0.25 rpm, 0.5 rpm, and 1 rpm. The orientation, as well as the rotation axis for all these cases, is illustrated in **Figure 4.3**.

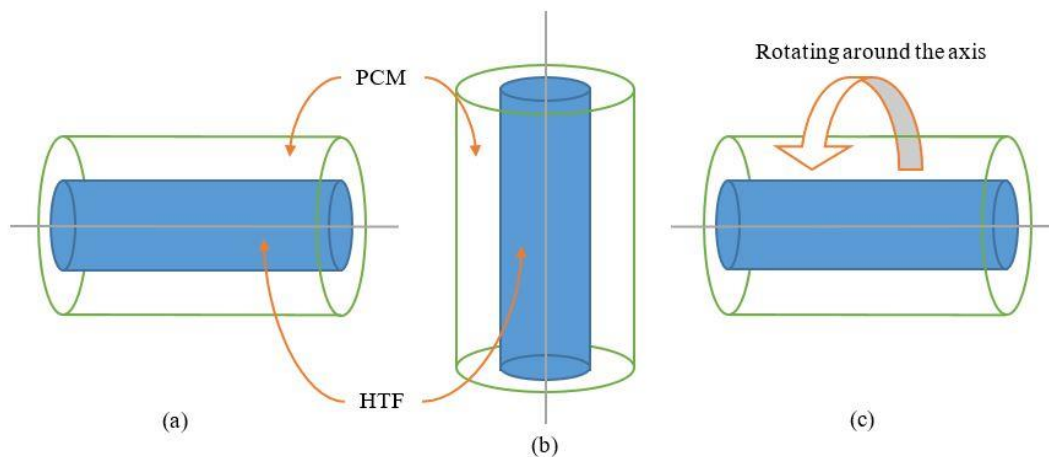


Figure 4.3: A shell-and-tube LHTES unit in (a) horizontal orientation, (b) vertical orientation and (c) horizontal orientation with rotation. PCM is stored in the shell (white) while HTF is allowed to flow into the tube (blue).

During charging, the hot water (heat transfer fluid, HTF) flows into the copper tube. Heat from the HTF is transferred through the copper tube to the phase change material (PCM) to store the thermal energy as a combination of sensible heat and latent heat. This caused the PCM to undergo phase change and melt. The charging process is set to run until all of the PCM has melted. The heat energy stored in the LHTES system is 766.78 kJ/kg and is the same for all cases.

While at discharging, cold water flows through the copper tube to remove heat from PCM. The PCM is solidified when heat is removed. The simulation of the discharging process is carried out after simulation of charging process has completed. Once started, the discharging process is continued until all of the PCM has solidified.

4.4 Effect of Orientation

Figure 4.4 shows the time evolution of melting of PCM for various orientation of LHTES system. It is observed that the horizontal steady orientation provides better heat transfer performance, indicated by the bigger melting fraction at the intermediate stage of charging process. However, towards the end of the charging process, the vertical with bottom inlet orientation reaches steady state first. This is followed closely by the horizontal steady orientation and lastly the vertical with top inlet orientation.

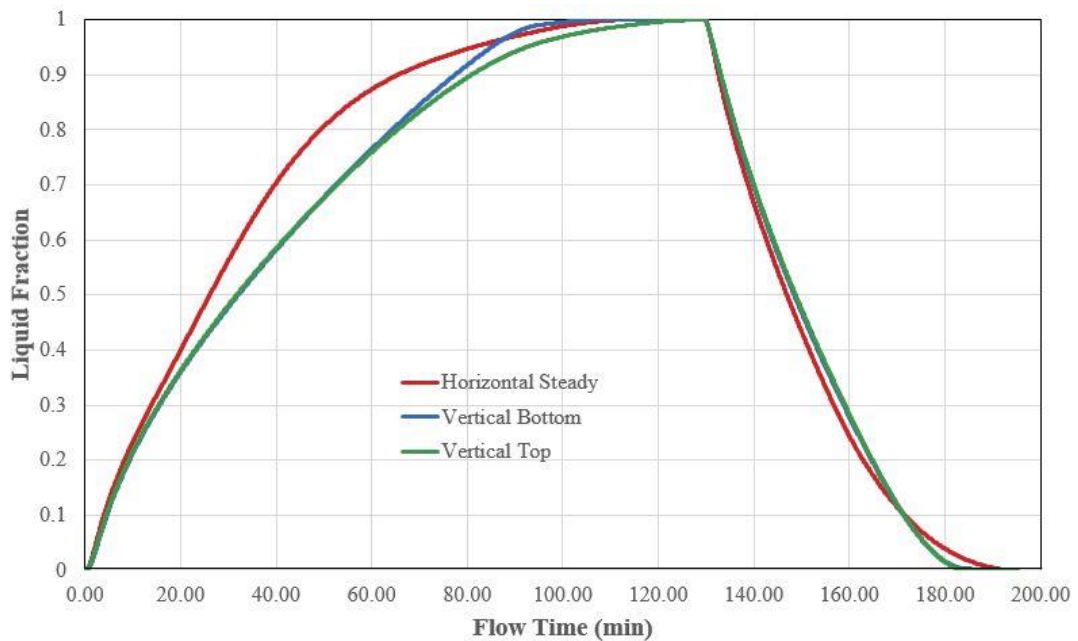


Figure 4.4: Graph of liquid fraction against flow time for horizontal steady, vertical with bottom inlet and vertical with top inlet.

This is attributed to the fact that effect of natural convection is acting along the length of the LHTES system in both the vertically oriented cases. On the other hand, in the horizontally oriented case, the effect of natural convection acts upwards, perpendicular to the length of the LHTES system. Therefore, heat is uniformly distributed in the cross section of both the vertically oriented cases. Yet, in the horizontally oriented case, heat is poorly distributed due to the effect of natural convection. This is clearly depicted in **Figures 4.5 – 4.7** which illustrates the liquid fraction distribution along the shell-and-tube LHTES system with different orientation after 1 hour of charging.

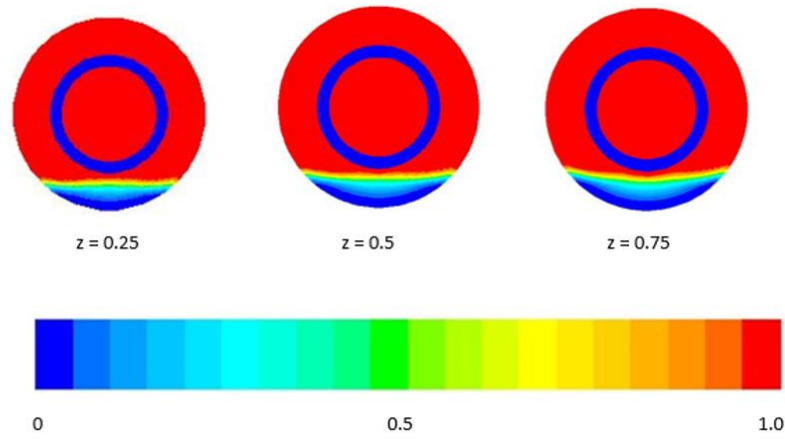


Figure 4.5: Liquid fraction of horizontal steady after 1 hour of charging.

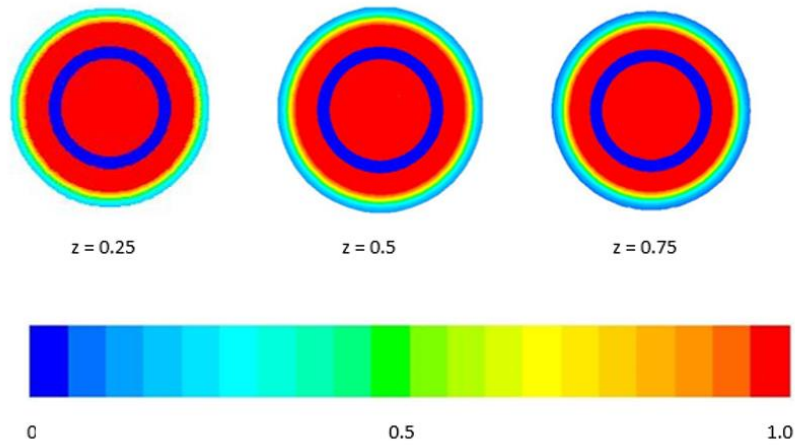


Figure 4.6: Liquid fraction of vertical steady with bottom inlet after 1 hour of charging.

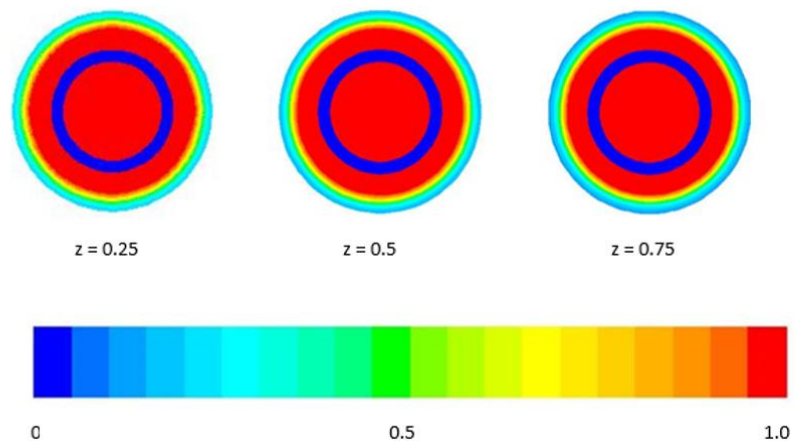


Figure 4.7: Liquid fraction of vertical steady with top inlet after 1 hour of charging.

In **Figures 4.5 – 4.10** and **Figures 4.12 – 4.21**, blue indicates of solids while red indicates liquids. The blue annular circle seen in the middle represents the copper tube. The region inside the blue circle should always be red as it represents the HTF which is always in a liquid state. The region outside the blue circle is the PCM.

Evidence poor heat distribution in the horizontally oriented LHTES system due to the effect of natural convection can be seen in **Figure 4.5** where a region of solid PCM accumulates at the bottom the shell. Natural convection is a phenomenon where a buoyancy effect occurs when less dense fluids rise leaving a vacant space. This vacant space is then filled with denser fluids. In the case of PCM, liquid PCM is less dense than solid PCM. Therefore, in the horizontally oriented LHTES system, the region above the copper tube melts faster than the region below the copper tube. On the other hand, in the vertically oriented LHTES systems, the region at the top should melt faster than the region at the bottom. However, due to the length of the LHTES system (1 metre), the effect of the natural convection on both the vertically oriented cases is not clearly shown in **Figures 4.6 – 4.7**.

During discharging, both the vertically oriented cases solidify at the same rate and reaches steady state faster than the horizontal steady case (**Figure 4.4**). **Figures 4.8 – 4.10** shows liquid fraction distribution along the shell-and-tube LHTES system with different orientation after 30 minutes of discharging. It is observed that both the vertically orientated cases have more uniform distribution of solid PCM than the horizontal steady orientation.

In the discharging process of the horizontal steady orientation of the LHTES system, similar scenario of the charging process is observed. **Figure 4.8** shows the region above the copper tube solidifies slower than the region below the copper tube due to the effect of natural convection as explain earlier. In addition to that, the uniform distribution of solids in **Figures 4.9 – 4.10** was also explained earlier.

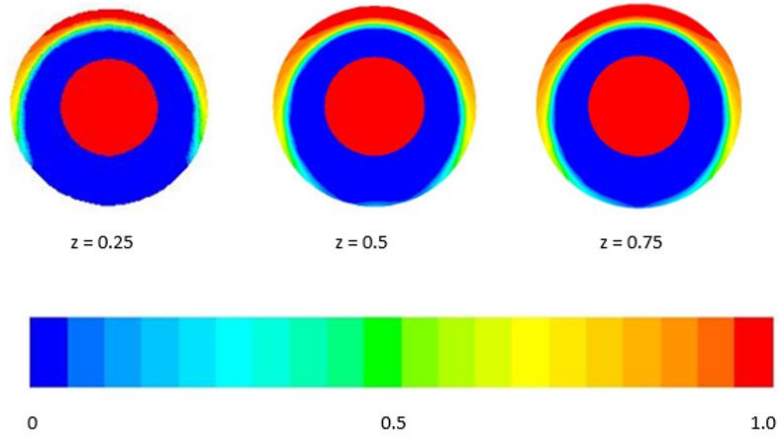


Figure 4.8: Liquid fraction of horizontal steady after 30 minutes of discharging.

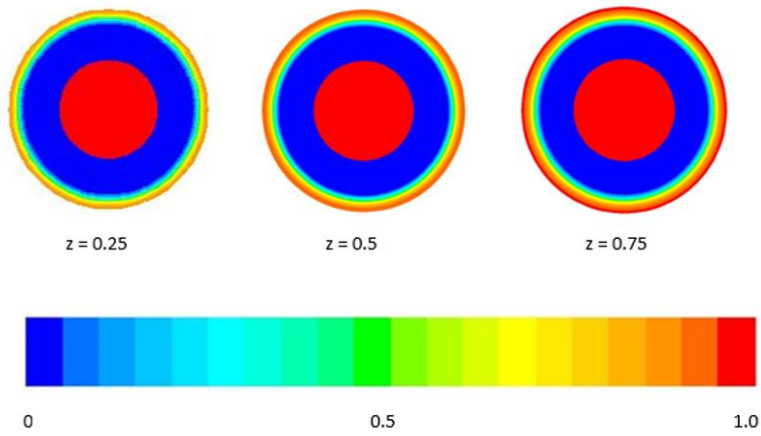


Figure 4.9: Liquid fraction of vertical steady with bottom inlet after 30 minutes of discharging.

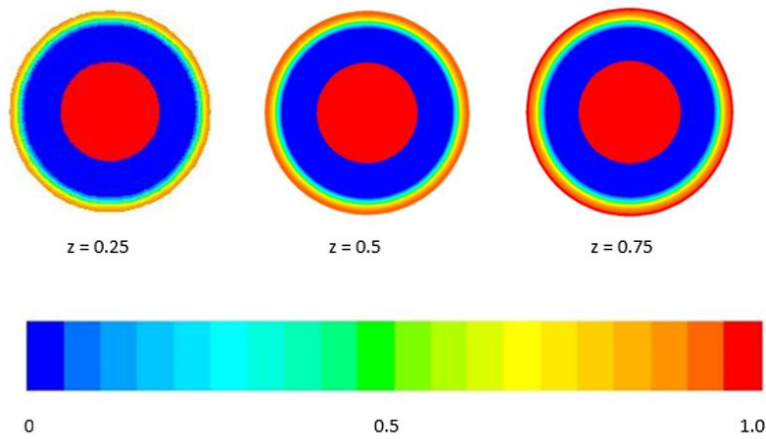


Figure 4.10: Liquid fraction of vertical steady with top inlet after 30 minutes of discharging.

4.5 Effect of Rotational Speed

In order to increase the heat transfer performance of the LHTES system, rotation of the system is introduced. The rotational effect will enhance the distribution of the buoyancy effect due to natural convection. The study of rotating LHTES system has been focused solely on the horizontal orientation only. LHTES system is rotated around its axis (the length of the shell-and-tube LHTES system).

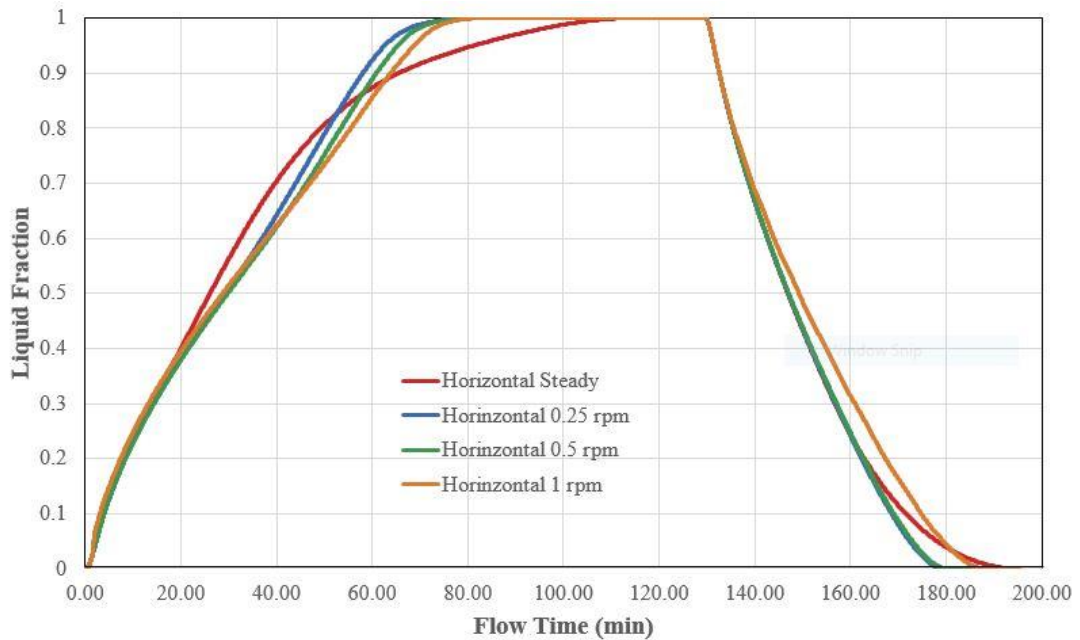


Figure 4.11: Graph of liquid fraction against flow time for horizontal steady, horizontal rotating at 0.25 rpm, horizontal rotating at 0.5 rpm and horizontal rotating at 1 rpm.

Figure 4.11 shows the time evolution of melting of PCM for the various rotational speed of LHTES system. It is observed that the stationary LHTES system provides better heat transfer performance at the intermediate stage of charging process, indicated by the bigger melting fraction. However, towards the end of the charging process, the rotating LHTES systems reaches steady state first. The rotating LHTES systems are fully charged approximately 30 minutes earlier than the stationary LHTES system. Apart from that, it is also observed that the slower the rotation of the LHTES system, the better heat transfer performance, shown by the bigger melting fraction.

As explained earlier, the effect of natural convection is that a buoyancy force is induced due to the variation in density of the fluids. In the case of stationary LHTES system (**Figure 4.12**), the buoyancy force is always acting in the same direction, upwards and perpendicular to the length of the LHTES system. On the other hand, when the LHTES system is rotating (**Figure 4.13 – 4.15**), the direction the buoyancy force is acting at is always shifting. When **Figure 4.12** is compared with **Figures 4.13 – 4.15**, the combined effect of natural convection and rotation which induce a more uniform heat distribution in the cross section of the rotating LHTES systems is seen.

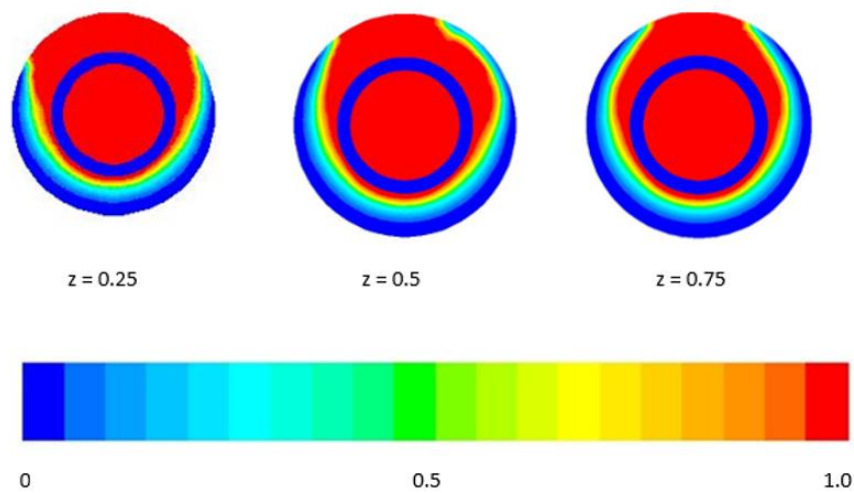


Figure 4.12: Liquid fraction of horizontal steady after 30 minutes of charging.

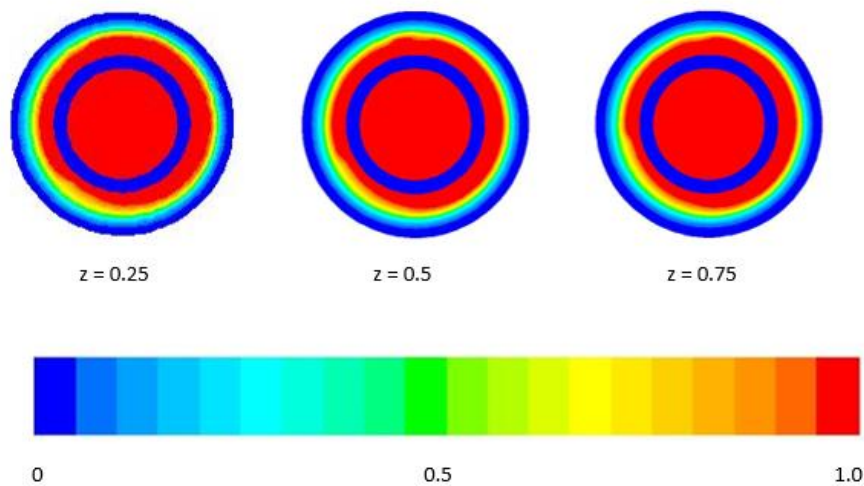


Figure 4.13: Liquid fraction of horizontal with 0.25 rpm after 30 minutes of charging.

Figures 4.16 – 4.18 shows liquid fraction distribution along the shell-and-tube LHTES system with different rotational speed after 1 hour of charging. The combined effect of natural convection and rotation is clearly portrayed by the yellow arc present throughout the length of the rotating LHTES systems.

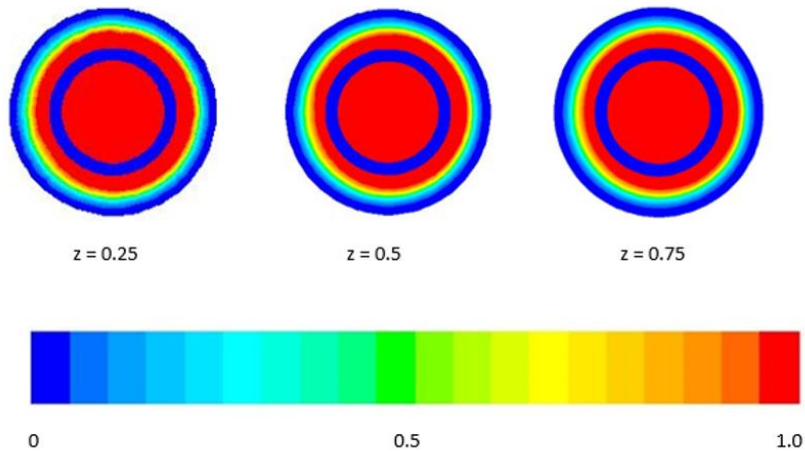


Figure 4.14: Liquid fraction of horizontal with 0.5 rpm after 30 minutes of charging.

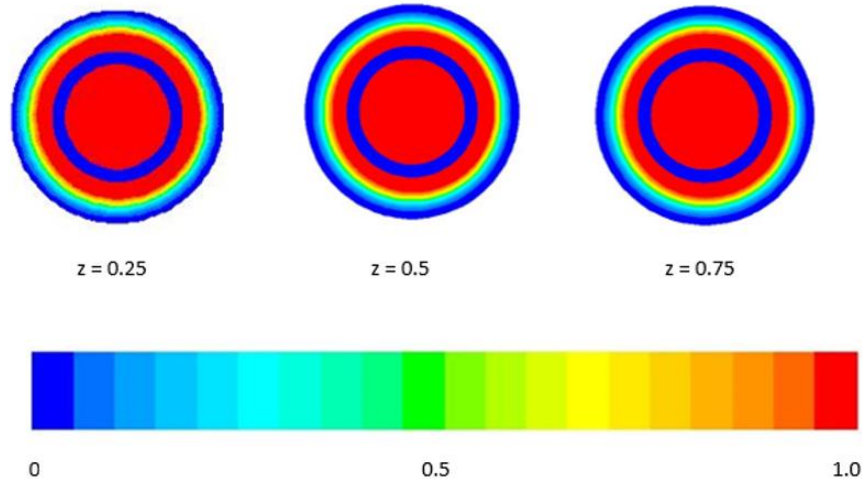


Figure 4.15: Liquid fraction of horizontal with 1 rpm after 30 minutes of charging.

The yellow arc in these figures proves that the effect of rotation results in the constant shifting of the direction the buoyancy force created by the natural convection. This further demonstrates that the effect of rotation induces uniform heat distribution in the cross section of the rotating LHTES systems. Consequently, the heat transfer performance of the rotating LHTES system increases. **Figures 4.16 – 4.18** also

confirms that the slower the rotational speed, the higher the rate of PCM melting, the higher the heat transfer performance.

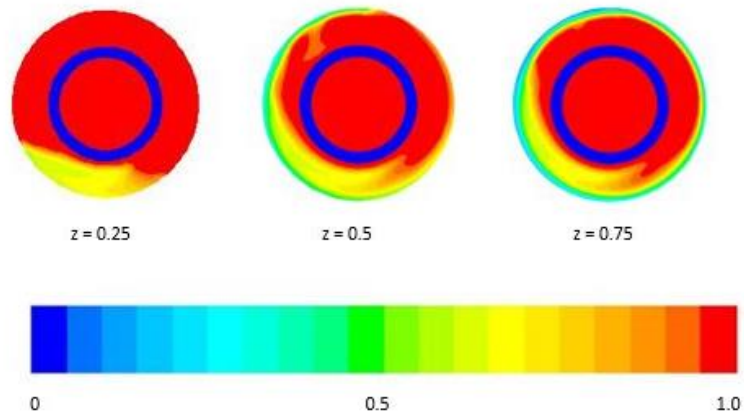


Figure 4.16: Liquid fraction of horizontal with 0.25 rpm after 1 hour of charging.

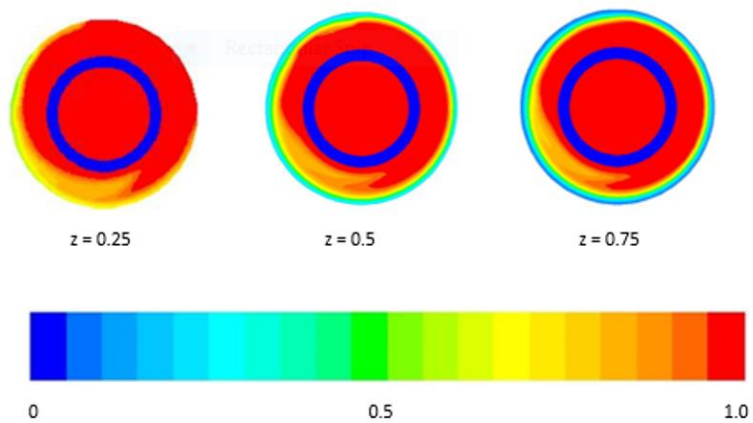


Figure 4.17: Liquid fraction of horizontal with 0.5 rpm after 1 hour of charging.

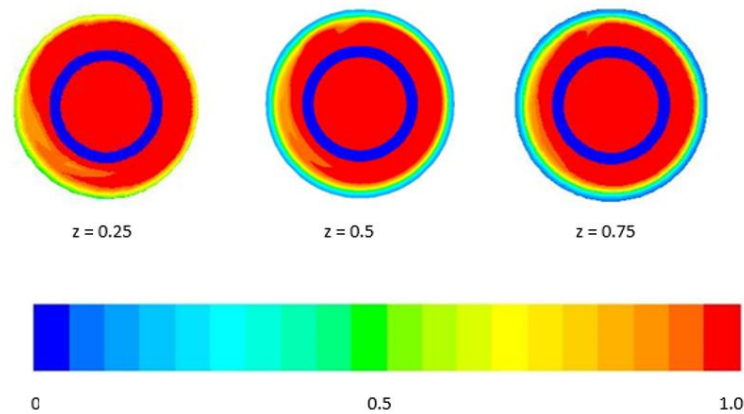


Figure 4.18: Liquid fraction of horizontal with 1 rpm after 1 hour of charging.

Referring back to **Figure 4.11**, the same observation is made during discharging which is the rotating LHTES systems yields better heat transfer performance than the stationary LHTES system. This is indicated by the bigger solidifying fraction in rotating LHTES systems. Additionally, the slower the rotation of the LHTES system, the better heat transfer performance, shown by the bigger solidifying fraction. However, the effect of rotation during discharging is less significant than the charging process. Rotating LHTES systems get fully discharged approximately 15 minutes earlier than stationary LHTES system. As explained earlier, the combined effect of rotation and natural convection creates a more uniform heat distribution in the cross section of the rotating LHTES systems. This is again observed in **Figure 4.19 – 4.21** which shows liquid fraction distribution along the shell-and-tube LHTES system with different rotational speed after 30 minutes of discharging.

When **Figure 4.8** is compared with **Figures 4.19 – 4.21**, the combined effect of natural convection and rotation which induce a more uniform heat distribution in the cross section of the rotating LHTES systems is seen. This shows that even though the time taken for discharging to be completed has not been significantly reduced, uniform distribution of the solid PCM is clearly seen in the rotating LHTES systems.

The combined effect of rotation and natural convection act as a catalyst in speeding up the charging and discharging process as observed in **Figures 4.12 – 4.21**. The increase in heat transfer performance of a rotating LHTES system during charging is substantially bigger than discharging. This is because natural convection dominates the heat transfer during charging while heat conduction dominates the heat transfer during discharging [22]. These results suggest that the rotating LHTES systems increase the heat transfer performance during charging and discharging. Therefore, it can be deduced that the rotating LHTES systems have the potential to be used to enhance the heat transfer performance during charging and discharging. However, further studies are needed to investigate the optimum rotational speed required by the LHTES system.

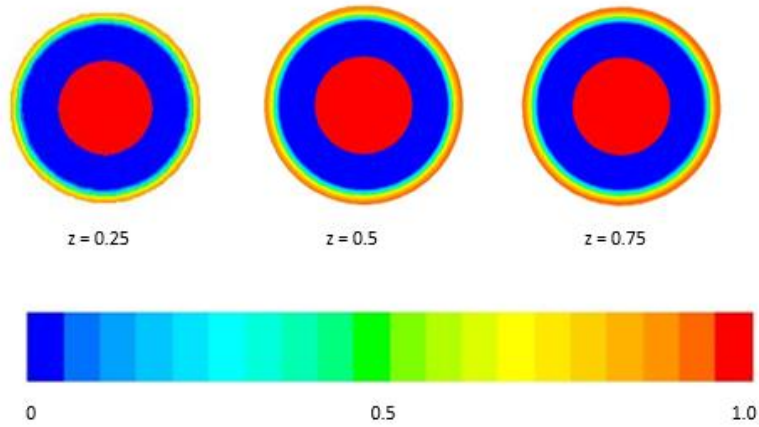


Figure 4.19: Liquid fraction of horizontal with 0.25 rpm after 30 minutes of discharging.

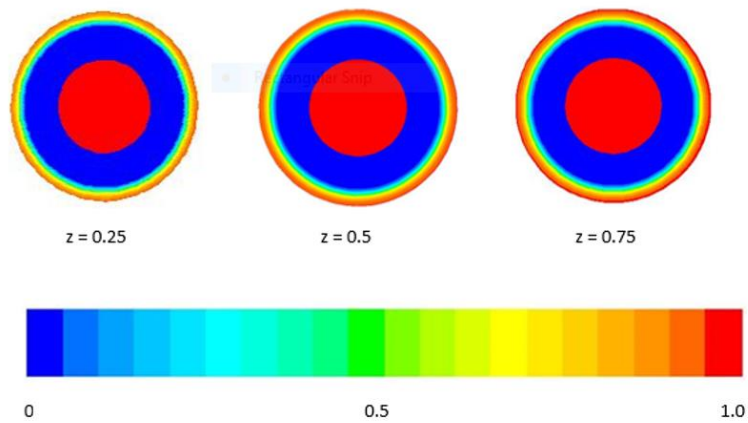


Figure 4.20: Liquid fraction of horizontal with 0.5 rpm after 30 minutes of discharging.

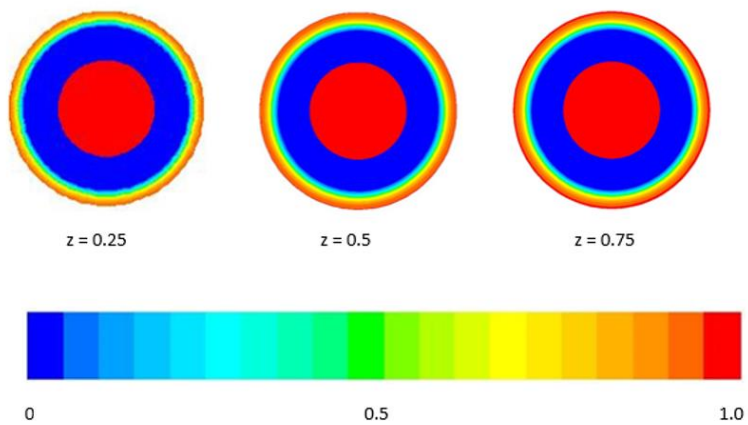


Figure 4.21: Liquid fraction of horizontal with 1 rpm after 30 minutes of discharging.

4.6 Rate of Heat Transfers

Figure 4.22 shows the time taken for charging and discharging process for all cases conducted in this study. From this bar chart, the comparison between cases can be done easily. It is observed that the rotating cases have better heat transfer performance compared to the non-rotating cases. This is indicated by the less time required by the rotating cases to complete one cycle of charging and discharging.

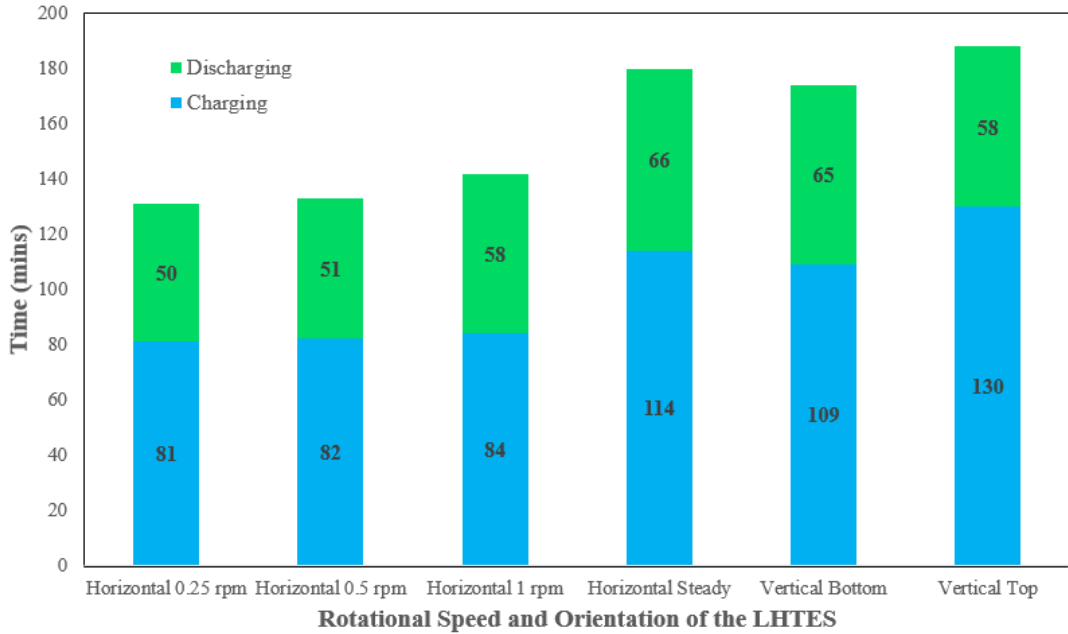


Figure 4.22: Time taken for charging and discharging process to be completed for all 6 cases.

The rate of heat transfer, i.e. $\dot{q} = q/t$, is evaluated by dividing the heat stored in the LHTES system (sub-chapter 3.4) against the time obtained from **Figure 4.22**. To simplify the calculations of the rate of heat transfer of the LHTES systems, it is assumed that the round trip efficiency of the system is 1. This indicates the heat loss in the LHTES system during the charging and discharging cycle has been neglected.

From **Table 4.1**, it is shown that by rotating the LHTES system, the rate of heat transfer has significantly improved during the charging process. The best performing rotating LHTES system in this study is the 0.25 rpm case, which boosts the charging rate by 41% and the discharging rate by 32%. The 0.5 rpm and 1 rpm cases improve the

charging rate by 39% and 36% respectively and the discharging rate of 29% and 14% respectively.

Table 4.1: Heat transfer rates for different cases.

Cases	Charging Process	Discharging Process
Vertical (Inlet Bottom)	0.117 kJ/kg.s	0.197 kJ/kg.s
Vertical (Inlet Top)	0.098 kJ/kg.s	0.220 kJ/kg.s
Horizontal Steady	0.112 kJ/kg.s	0.194 kJ/kg.s
Horizontal 0.25 rpm	0.158 kJ/kg.s	0.256 kJ/kg.s
Horizontal 0.5 rpm	0.156 kJ/kg.s	0.251 kJ/kg.s
Horizontal 1 rpm	0.152 kJ/kg.s	0.220 kJ/kg.s

CHAPTER 5:

CONCLUSION AND RECOMMENDATION

As a conclusion, computational fluid dynamics (CFD) simulation has been conducted on a rotating latent heat thermal energy storage (LHTES) system. The effect of orientation of the LHTES system as well as the rotation effect on the heat transfer performance of the LHTES system has been investigated. By analysing the results, the following conclusions can be made:

- Vertically oriented LHTES system has more uniform heat distribution, hence the heat transfer performance is stronger than horizontally oriented LHTES system.
- Rotating the horizontally oriented LHTES system enhance its heat transfer performance. This is achieved because the effect of natural convection is uniformly distributed in the cross-section due to the effect of rotation.
- The slower the rotation of the horizontally oriented LHTES system, the better the heat distribution in the cross-section. Hence, resulting in better the heat transfer performance.
- Significant improvement of heat transfer performance due to the effect of rotation is only observed during the charging process. This is because natural convection is the biggest influencing heat transfer mode during the charging process. Whereas conduction mode of heat transfer dominates the discharging process.

The objectives of this project which is to formulate a model of a rotating latent heat storage (LHTES) has been achieved. Apart from that the investigate the heat transfer performance of the rotating LHTES and its key parameters has been successfully completed.

Nevertheless, further numerical and experimental work has to be conducted to concretely prove the hypothesis of this project. It is advised the experimental work is given more attention as the numerical method used in this project is very time-consuming. This is mainly due to the insufficient computational power provided for this project. However, if the numerical solution is still preferred, it is advisable that the study focuses on determining the optimum rotational speed. The optimum rotational speed is speculated to range from 0.01 – 0.5 rpm based on the results obtained in this study.

REFERENCE

- [1] International Energy Agency, “World Energy Outlook 2015,” 2015.
- [2] International Energy Agency, “World Energy Outlook 2015 Factsheet,” 2015.
- [3] B. Xu, P. Li, and C. Chan, “Application of phase change materials for thermal energy storage in concentrated solar thermal power plants: A review to recent developments,” *Appl. Energy*, vol. 160, pp. 286–307, 2015.
- [4] International Energy Agency, “Solar.” [Online]. Available: <http://www.iea.org/topics/renewables/subtopics/solar/>. [Accessed: 31-Mar-2016].
- [5] A. Sharma, V. V. Tyagi, C. R. Chen, and D. Buddhi, “Review on thermal energy storage with phase change materials and applications,” *Renew. Sustain. Energy Rev.*, vol. 13, no. 2, pp. 318–345, 2009.
- [6] S. Kuravi, J. Trahan, D. Y. Goswami, M. M. Rahman, and E. K. Stefanakos, “Thermal energy storage technologies and systems for concentrating solar power plants,” *Prog. Energy Combust. Sci.*, vol. 39, no. 4, pp. 285–319, Aug. 2013.
- [7] International Energy Agency, “Technology Roadmap: Concentrating Solar Power,” 2010.
- [8] ETSAP/IRENA, “Thermal Energy Storage. Technology Brief,” no. January, p. 24, 2013.
- [9] M. M. Farid, A. M. Khudhair, S. A. K. Razack, and S. Al-Hallaj, “A review on phase change energy storage: Materials and applications,” *Energy Convers. Manag.*, vol. 45, no. 9–10, pp. 1597–1615, 2004.

- [10] R. E. Murray and D. Groulx, “Experimental study of the phase change and energy characteristics inside a cylindrical latent heat energy storage system: Part 1 consecutive charging and discharging,” *Renew. Energy*, vol. 62, pp. 571–581, 2014.
- [11] R. Velraj, R. V. Seeniraj, B. Hafner, C. Faber, and K. Schwarzer, “HEAT TRANSFER ENHANCEMENT IN A LATENT HEAT STORAGE SYSTEM,” *Sol. Energy*, vol. 65, no. 3, pp. 171–180, 1999.
- [12] Y. B. Tao and Y. L. He, “Effects of natural convection on latent heat storage performance of salt in a horizontal concentric tube,” *Appl. Energy*, vol. 143, pp. 38–46, 2015.
- [13] M. Lacroix, “Numerical simulation of a shell-and-tube latent heat thermal energy storage unit,” *Solar Energy*, vol. 50, no. 4, pp. 357–367, 1993.
- [14] H. A. Adine and H. El Qarnia, “Numerical analysis of the thermal behaviour of a shell-and-tube heat storage unit using phase change materials,” *Appl. Math. Model.*, vol. 33, no. 4, pp. 2132–2144, 2009.
- [15] Y. A. Çengel and A. J. Ghajar, *Heat and mass transfer: fundamentals & applications*, Fourth. Singapore: McGraw-Hill, 2015.
- [16] Y. A. Çengel and M. A. Boles, *Thermodynamics: an Engineering Approach*, Seventh., vol. 8, no. 8. Singapore: McGraw-Hill, 2015.
- [17] A. F. Regin, S. C. Solanki, and J. S. Saini, “Latent heat thermal energy storage using cylindrical capsule: Numerical and experimental investigations,” *Renew. Energy*, vol. 31, no. 13, pp. 2025–2041, 2006.
- [18] S. M. Hasnain, “Review on sustainable thermal energy storage technologies, Part I: heat storage materials and techniques,” *Energy Convers. Manag.*, vol. 39, no. 11, pp. 1127–1138, 1998.
- [19] T. Nomura, N. Okinaka, and T. Akiyama, “Technology of Latent Heat Storage for High Temperature Application: A Review,” *Isij Int.*, vol. 50, no. 9, pp. 1229–1239, 2010.

- [20] B. Gibbs and S. Hassan, "DSC study of technical grade phase change heat storage materials for solar heating," in *Journal Of Solar Energy Engineering-Transactions Of The Asme*, 1995, vol. 2, pp. 1053–1062.
- [21] "n-octadecane - Wolfram|Alpha." [Online]. Available: <http://www.wolframalpha.com/input/?i=n-octadecane>. [Accessed: 01-Apr-2016].
- [22] J. C. Kurnia, A. P. Sasmito, S. V. Jangam, and A. S. Mujumdar, "Improved design for heat transfer performance of a novel phase change material (PCM) thermal energy storage (TES)," *Appl. Therm. Eng.*, vol. 50, no. 1, pp. 896–907, 2013.